Novel polyurethane-based thermosensitive hydrogels as drug release and tissue engineering platforms: design and in vitro characterization

Novel polyurethane-based thermosensitive hydrogels as drug release and tissue engineering platforms: design and in vitro characterization.

Monica Boffito, Emilia Gioffredi, Valeria Chiono, Stefano Calzone, Elia Ranzato, Simona Martinotti, Gianluca Ciardelli*

[*] Prof. Gianluca Ciardelli

Department of Mechanical and Aerospace Engineering

Politecnico di Torino

Corso Duca degli Abruzzi 24, 10129 Turin (ITALY)

Tel: (+39) 0110906919

Fax: (+39) 011 0906999

E-mail address: gianluca.ciardelli@polito.it

Prof. Gianluca Ciardelli

CNR-IPCF UOS Pisa

Via Moruzzi 1, 56124 Pisa (ITALY)

Monica Boffito

Department of Mechanical and Aerospace Engineering

Politecnico di Torino

Corso Duca degli Abruzzi 24, 10129 Turin (ITALY)

Emilia Gioffredi

Department of Mechanical and Aerospace Engineering

Politecnico di Torino

Corso Duca degli Abruzzi 24, 10129 Turin (ITALY)

Valeria Chiono

Department of Mechanical and Aerospace Engineering

Politecnico di Torino

Corso Duca degli Abruzzi 24, 10129 Turin (ITALY)

Stefano Calzone

Department of Mechanical and Aerospace Engineering

Politecnico di Torino

Corso Duca degli Abruzzi 24, 10129 Turin (ITALY)

Elia Ranzato

Dipartimento di Scienze e Innovazione Tecnologica

University of Piemonte Orientale,

Viale T. Michel 11, 15121 Alessandria (ITALY)

Simona Martinotti

Dipartimento di Scienze e Innovazione Tecnologica

University of Piemonte Orientale,

Viale T. Michel 11, 15121 Alessandria (ITALY)

Abstract

Poloxamer P407 (P407) is a FDA approved triblock copolymer; its hydrogels show fast dissolution in aqueous environment and weak mechanical strength, limiting their *in vivo* application. In this work, an amphiphilic poly(ether urethane) (NHP407) was synthesized from P407, an aliphatic diisocyanate (1,6-hexanediisocyanate) and an amino acid derived diol (N-Boc serinol). NHP407 solutions in water-based media were able to form biocompatible injectable thermosensitive hydrogels with a lower critical gelation temperature (LCGT) behavior, having lower critical gelation concentration (6%w/v *versus* 18%w/v), superior gel strength (G' at 37°C about 40000 Pa *versus* 10000 Pa), faster gelation kinetics (< 5 min *versus* 15-30 min) and higher stability at physiological conditions (28 days *versus* 5 days), compared to P407 hydrogels. Dissolution rate (in phosphate buffered saline, PBS at 37°C), permeability to nutrients (studied using fluorescein isothiocyanate-dextran -FD4- model molecule) and gel strength increased whereas PBS absorption at 37°C decreased as a function of NHP407 hydrogel concentration from 10 to 20%w/v.

By varying the concentration, NHP407 hydrogels were thus prepared with different properties which could suit specific applications, such as *in situ* drug/cell delivery or bioprinting of scaffolds. Moreover, deprotected amino groups in NHP407 could be exploited for the grafting of bioactive molecules obtaining biomimetic hydrogels.

Keywords: polyurethane hydrogels, Poloxamer, thermosensitive hydrogels, tissue engineering, drug release, bioprinting

Introduction

Hydrogels are three-dimensional (3D) hydrophilic polymer networks able to retain large amounts of biological fluids, and characterized by soft and rubbery consistence, enabling them to mimic specific aspects of tissue microenvironments.[1–5] Hydrogels have been widely investigated in regenerative medicine owing to their highly tunable physico-chemical and mechanical properties that allow them to provide a soft tissue-like environment for cells with controlled diffusion of nutrients, molecules and cellular waste through the elastic hydrogel network.[2,5–8] They have also been used for drug delivery due to their biocompatibility and permeability.[4,5]

Recently, thermosensitive polymer-based injectable in situ forming hydrogels have been investigated for biomedical applications. The term “thermosensitive” defines the capability of these hydrogels to change their physico-mechanical properties in response to temperature changes. The sol-gel transition, indeed, is driven exclusively by temperature and does not require the addition of potentially toxic chemical reagents, such as cross-linkers, organic solvents or catalysts. Thermosensitive hydrogels can be categorized into upper critical gelation temperature hydrogels (UCGT) and lower critical gelation temperature hydrogels (LCGT), forming a gel by cooling below UCGT or heating above LCGT, respectively. Hydrogels with LCGT behavior have gained increasing attention as carriers for cells, bioactive molecules and drugs due to many advantages, such as: (i) the possibility to encapsulate cells and molecules in mild conditions by dispersion in polymer aqueous solution a low temperature followed by gelation in physiological conditions, (ii) the easy application (minimally invasive injection in the sol state followed by gelation in situ) and (iii) the ability to assume the desired shape (capability to completely fill any body cavities or defects prior to complete gelation).[4,8–11]

Poloxamers are non-toxic FDA approved poly(ethylene oxide)/poly(propylene oxide)/poly(ethylene oxide) (PEO-PPO-PPO) triblock copolymers, which hydrogels belong

to the family of LCGT hydrogels. The thermosensitive behavior of Poloxamer-based aqueous solutions has paved the way to their application as drug and/or cell carriers.[12–14] However, Poloxamer-based hydrogel disadvantages, such as fast dissolution, high permeability in aqueous environment and weak mechanical strength, have limited their application in the biomedical field.[15,16] Providing Poloxamer with functional groups for chemical crosslinking during gelation or increasing its molecular weight are effective strategies to enhance hydrogel stability in a water based environment.[15–18] In 2006, Sun et al. reported a Poloxamer-based disulfide multiblock copolymer with increased gel stability in aqueous environment and a thiol-concentration dependent degradation and drug release kinetics.[17] More recently, Niu and colleagues synthesized an acrylate/thiol modified Poloxamer P407, which solutions were able to undergo chemical gelation in physiological conditions as a consequence of the spontaneous reaction between thiol and acrylate.[15] With the final aim of decreasing the concentration necessary to induce the sol-to-gel transition at 37°C, Volkmer et al. successfully chain extended Pluronic P123 with 1,6-diisocyanatehexane (HDI), 1,4-butane diisocyanate (BDI) and hydrogenated diphenylmethane diisocyanate (H_{12}MDI).[16] Similarly, Cohn and colleagues chain extended Pluronic F127 with HDI, demonstrating the effectiveness of chain extension in remarkably increased hydrogel viscosity and critical gelation concentration (CGC, minimal concentration required to observe a sol-to-gel transition) compared to F127-based hydrogels.[18] Similar results were reported in 2014 by Loh et al. that synthesized a poly(ether carbonate urethane) from Pluronic F127 and poly(polytetrahydrofurancarobonate) (PTHF) diol, using HDI as coupling agent.[19] In this study, the chain extension strategy was improved by synthesizing a poly(ether urethane) (PEU) through a two step procedure, based on a first reaction of Poloxamer P407 and HDI, followed by a second reaction between the formed prepolymer and an amino acid derived diol (N-BOC serinol). The Boc-protected amino groups are available for further functionalization with proteins or peptides after deprotection in acidic

conditions.[20] Aqueous solutions of the synthesized PEU (acronym NHP407) and Poloxamer P407 were both characterized in terms of micellization potential, gelation temperature, time and kinetics, and stability in water environment to assess the capability of the newly developed hydrogels to overcome Poloxamer P407 gel drawbacks. In addition, hydrogel injectability, cytotoxicity and permeability to nutrients were tested in the perspective of their application in the biomedical field as injectable *in situ* gel-forming systems or scaffold forming materials in bioprinting technology.

Materials and methods

Materials

Poloxamer P407 (P407, M_n=12600 Da, 70%w/w PEO), 1,6-hexanediisocyanate (HDI), dibutyltindilaurate (DBTDL) and N-Boc serinol were purchased from Sigma Aldrich, Italy. P407 and N-Boc Serinol were dried overnight under reduced pressure at room temperature to remove residual water before use. HDI was distilled under reduced pressure before use. All solvents were purchased from Sigma Aldrich, Italy in the analytical grade.

Synthesis of Poloxamer-based poly(ether urethane)

Poloxamer-based PEU was synthesized through a two-step procedure in inert atmosphere using anhydrous 1,2 dichloroethane (DCE) as solvent and starting from P407 as macrodiol, HDI and N-Boc serinol as chain extender.

P407 (20%w/v in DCE) was reacted with HDI (1:2 molar ratio with respect to P407) for 2.5 h at 80°C, in the presence of the catalyst (DBTDL, 0.1%w/w respect to P407) to form the prepolymer. In the second step, N-Boc serinol was added (3%w/v in DCE, 1:1 molar ratio with respect to P407) and the reaction (1.5 h at 60°C) was stopped with methanol. The polymer was collected by precipitation in petroleum ether (4:1 volume ratio with respect to

DCE), purified by dissolution in DCE (20%w/v) followed by precipitation in diethyl ether and methanol (98:2 v:v) (5:1 volume ratio with respect to DCE) and finally washed in diethyl ether (5 g x 100 ml). The obtained polymer was dried overnight under vacuum at room temperature, grinded and kept in nitrogen atmosphere at 5°C.

The synthesized PEU has NHP407 acronym, where the first letter (N) indicates the chain extender, H corresponds to HDI, while P407 refers to Poloxamer P407.

PEU chemical characterization

Infrared spectroscopy and size exclusion chromatography (SEC)

Attenuated Total Reflectance Fourier Transform Infrared (ATR-FT-IR) Spectra of P407 and NHP407 powder were obtained at room temperature in the spectral range from 4000 to 600 cm^{-1} using a Perkin Elmer Spectrum 100 equipped with an ATR accessory (UATR KRS5) with diamond crystal. Each spectrum, obtained as a result of 16 scans with a resolution of 4 cm^{-1}, was analyzed using the Perkin Elmer Spectrum Software.

Size Exclusion Chromatography (SEC) (Agilent Technologies 1200 Series, USA) was conducted according to a previously reported protocol.[21]

Hydrogel characterization

Sol-gel system preparation

Sol-gel systems were prepared by NHP407 or P407 solubilization at predefined concentrations (%w/v) in an aqueous medium (phosphate buffered saline (PBS, pH 7.4) or Dulbecco's Modified Eagle Medium (DMEM) with high glucose content (Sigma-Aldrich, Italy)) at 5°C overnight to avoid micellization and/or gelation during solution preparation.

Dynamic Light Scattering (DLS)

The average hydrodynamic diameter of the polymeric structures present in NHP407 and P407 solutions (0.5 and 1%w/v in PBS) was estimated by DLS (Zetasizer Nano S90, Malvern Instruments, UK) at different temperatures (25, 30, 37 and 45°C; equilibration time 2 minutes), according to the method reported by Pradal et al.[22] Micelle size was calculated as the mean value of three measurements. Due to the turbidity of the gel forming solutions, only dilute solutions unable to gel were investigated to study the mechanism of polymeric structure formation as a function of solution concentration and temperature.

Critical micellar temperature (CMT) estimation

CMT was studied by adding the 1,6-diphenly-1,3,5-hexatriene (DPH) fluorescent dye ($4 \cdot 10^{-4}$ M in methanol) to NHP407- and P407-based solutions (0.1, 0.5, 1, 3, 5 and 6%w/v in PBS) as a marker for micellization. UV-Vis absorption spectroscopy (PerkinElmer Lambda 25 UV/VIS Spectrometer) was used to evaluate micellization since DPH absorbance intensity at 350-360 nm increases as it is solubilized into the hydrophobic micelle core.[23] The analysis was conducted in the temperature range from 5 to 40°C at a rate of 1°C/step (with an equilibration time of 5 minutes at each temperature). CMT was estimated from the intensity of the UV-Vis absorption peak centered at 356 nm according to the protocol reported by Alexandridis et al.[23]

Tube Inverting Test

Tube inverting test was conducted on P407 (concentrations ranging from 16%w/v to 35%w/v) and NHP407 (concentrations ranging from 3%w/v to 25%w/v) solutions in PBS (1.5ml in a Bijoux sample container (Sigma-Aldrich, Italy) with an inner diameter of 17 mm) to characterize their sol-gel-sol phase transition.[24–26] Each sample was subjected to a controlled temperature increase from 5 to 70°C. Each step consisted of a 1°C temperature

increase, followed by temperature maintenance for 5 minutes and tube inversion, that allowed the visual inspection of the sol-gel-sol transition. Conditions of sol and gel were defined as “flow liquid sol” and “no flow solid gel” in 30s, respectively.

Gelation time in physiological conditions

Hydrogel gelation potential in physiological conditions was studied by NHP407 and P407 solution (0.5 ml; 5, 6, 7, 8, 9, 10, 15, 18, 20 and 25%w/v in PBS) incubation at 37°C (IKA KS-4000i control) for different times (5, 10, 15, 30, 45, 60, 90, 120, 180, 240, 300 and 360 min), followed by vial inversion Conditions of sol and gel were defined as “flow liquid sol” and “no flow solid gel” in 30s, respectively.

Rheological tests

Rheological tests on NHP407 and P407 solutions in PBS were performed by using a stress-controlled rheometer (MCR302, Anton Paar GmbH) equipped with a 25 mm parallel plate geometry. Temperature control was guaranteed by a Peltier system.

Temperature ramp tests at 1°C/min and constant shear rate (10 s^{-1}) were carried out to study the sol-to-gel transition (temperature ranging from 0 to 40°C). The yield stress (YS) was evaluated at 37°C by means of strain sweep tests (frequency=10 Hz, strain from 0.01 to 500%), while Small Amplitude Oscillatory Shear (SAOS) tests were conducted to check the viscoelastic properties of the gels (frequency sweep tests, frequency from 0.1 to 100 rad/s, strain=0.1%, 37, 40 and 42°C for NHP407 hydrogels with 15 and 20%w/v concentrations; 37, 40, 42, 45 and 50°C for NHP407 hydrogel with10%w/v concentration).

For each analysis, the sample was poured on the lower plate in sol phase at 0°C, heated at the chosen temperature, maintained in quiescent conditions for 15 minutes to reach the thermal stability and then tested.

Hydrogel stability and degradation

Stability and degradation tests were carried out on NHP407- (10, 15 and 20%w/v) and P407-based (20%w/v) hydrogels (1 ml). The prepared solutions were weighted (W_{gel_i}) and incubated at 37°C for 30 min to induce gelation before test beginning. Then, 2 ml of PBS were added to each vial. At predefined time intervals (3h, 6h, 1d, 3d, 7d, 14d and 28d), 3 samples were taken and weighted (W_{gel_f}) after removal of the residual PBS. The gels were then freeze dried (Martin Christ ALPHA 2-4 LSC) and again weighted ($W_{freeze\ dried\ gel\_f}$). Control gels (non-incubated in PBS) were also freeze dried and weighted ($W_{freeze\ dried\ gel\_i}$). PBS absorption and hydrogel degradation were estimated according to the following equations (**Eq.1** and **2**):

$$PBS\ absorption\ (\%) = \frac{(w_{gel\_f} - w_{gel\_i}) \cdot 100}{w_{gel\_f}} \qquad \text{Eq. (1)}$$

$$Hydrogel\ degradation\ (\%) = \frac{(w_{freeze\ dried\ gel\_i} - w_{freeze\ dried\ gel_f}) \cdot 100}{w_{freeze\ dried\ gel\_i}} \qquad \text{Eq. (2)}$$

Permeability test

Permeability studies were performed to assess nutrient transport across the hydrogel. Fluorescein isothiocyanate-dextran (FD4, M_w 3000-5000 g/mol; Sigma-Aldrich, Italy) is generally used as a model of nutrients since its Stokes radius (14 Å) is higher than that of nutrients (glucose and NaCl have a Stokes radius of 3.8 and 1.4 Å, respectively).[27]

After gelation at 37°C for 30 minutes, NHP407-based hydrogels (10, 15 and 20%w/v, 1 ml) were added with 1 ml of a FD4 solution in PBS (1 mg/ml) and incubated at 37°C. At predefined time steps (1, 7, 24, 48, 72 and 168 h), 3 samples were taken and the absorbance of the residual FD4 solution was measured by UV-Vis spectroscopy (PerkinElmer Lambda 25 UV/VIS Spectrometer) in the 350-600 nm range to measure the intensity of FD4 main

absorption peak at 493 nm. The amount of FD4 absorbed by the hydrogel was defined as the difference between the starting and the residual FD4 content in the solution incubated with the samples. The amount of FD4 in each sample was calculated by referring to a calibration curve based on FD4/PBS standards with well-defined concentrations (0.05, 0.1, 0.25, 0.5 and 0.75 mg/ml).

Hydrogel injectability

The injectability of NHP407 solutions and hydrogels with 10, 15 and 20%w/v concentrations was evaluated by using a volumetric pump (World Precision Instruments, Aladdin-1000) equipped with a traditional 2.5 ml plastic syringe. Injectability was tested by using two needles (6.3 mm length), differing in internal diameter (0.20 or 0.25 mm) (Iscra Dielectric S.r.l., Italy). The tests were carried out at four different flow rates (3, 5, 8 and 10 ml/h) at 5, 25 and 37°C.

The capability of the hydrogel to gel *in situ* was evaluated as reported by Ma et al.[28] In detail, P407 (20%w/v) and NHP407 (10, 15 and 20%w/v) solutions in PBS containing 0.5%w/v Brilliant Blue (Sigma Aldrich, Italy) were prepared at 5°C and, then, injected into a beaker containing 37°C distilled water.

The qualitative behavior of the injected hydrogels was evaluated by visual inspection.

Biological tests

All reagents were from Sigma-Aldrich, Italy, unless otherwise indicated.

Cell culture

Three different cell types were used:

- HaCaT immortalized human skin keratinocytes, mimicking many properties of normal epidermal keratinocytes.[29]

- C_2C_{12} immortalized mouse myoblast cell line.[30]
- 46 BR.1N human fibroblast cell line obtained from European Collection of Cell Cultures (ECACC). This cell line was originally derived from the skin of an individual with hypo-gammaglobulinemia and immortalized by transfection with the plasmid pSV3neo, expressing SV40 T-antigen.[31]

Cells were maintained at 37°C, 5% CO_2, in DMEM supplemented with 10% fetal bovine serum (FBS) and antibiotic mixture (1% penicillin-streptomycin) and glutamine.

Sample preparation

NHP407 and P407 solutions with 20%w/v concentration were prepared according to the previously described protocol. The obtained solutions were subjected to gelation at 37°C after deposition in a 6-multiwell plate (0.3 g/well) and sterilized before use by exposure to UV light for approx. 20 minutes.

Cytotoxicity test

Hydrogel cytotoxicity was assessed on extracts of the biomaterial in complete medium. Briefly, extracts were obtained by incubating the hydrogel into complete cell growth medium (DMEM supplemented with 10% FBS, glutamine (290µg/ml), penicillin (100U/ml) and streptomycin (100µg/ml)) at a concentration of 0.1 g/ml for 24 hours at 37°C. The obtained hydrogel extracts were supplemented to subconfluent cell cultures (20000 cell/well, 96-well plates) on conventional tissue culture plates. After 24 hours, the medium was removed and cells were gently washed with PBS, stained for 10 min with 0.5% crystal violet in 145 mmol/L NaCl, 0.5% formal saline, 50% ethanol, and washed thrice with water. Crystal violet was eluted from cells with 33% acetic acid and the absorbance of the supernatants was measured at 540 nm in a microplate reader (Infinite 200 Pro, Tecan, Wien, Austria).[32]

Statistical analysis

Results are reported as mean ± standard deviation.

Statistical analysis was performed using GraphPad Prism version 6.00 for Mac OS X (GraphPad Software, La Jolla California USA, www.graphpad.com). Two-way ANOVA analysis followed by Tukey's multiple comparison test were used to compare results. The statistical significance of each comparison was assessed according to **Table 1**.

Table 1

Results

PEU chemical characterization

The chemical structure of the synthesized PEU was analyzed by ATR-FTIR spectroscopy. **Figure1** reports ATR-FTIR spectra of P407 and NHP407 powder.

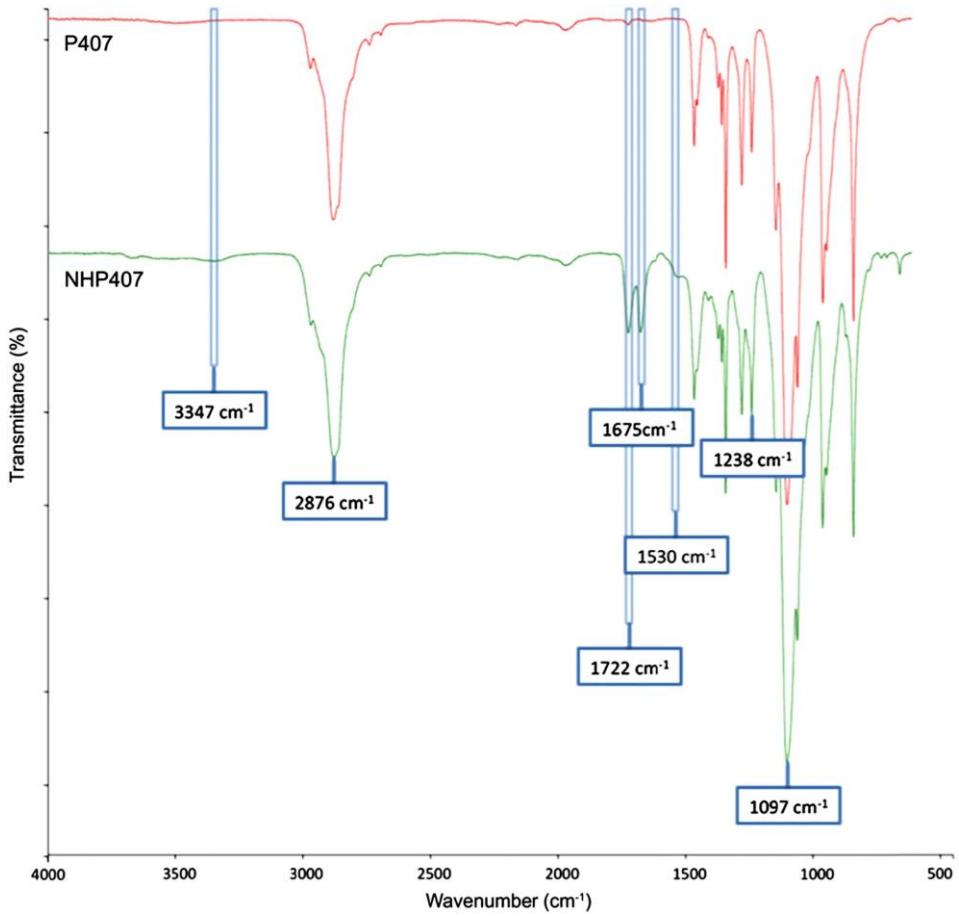

Figure 1. ATR-FTIR spectra of P407 (red) and NHP407 (green). Differences between the two spectra, proving the successful NHP407 synthesis, are highlighted at 3347, 1722, 1675 and 1530 cm^{-1}. The peaks at 2876, 1238 and 1097 cm^{-1} are typical of P407 structure.

P407 ATR-FTIR spectrum showed the characteristic absorption peaks of CH_2 stretching vibrations (2876 cm^{-1}) and CH_2 rocking and C-O-C stretching vibrations (1250-1000 cm^{-1}), due to the repeated $–OCH_2CH_2$ units of PEO.

NHP407 ATR-FTIR spectrum indicated the successful synthesis of a polyurethane incorporating P407 blocks: beside the above described typical absorption bands of P407, new bands were detected at 1722 cm^{-1} and 1675 cm^{-1} attributed to the stretching vibration of free and bound carbonyl groups (C=O) (amide I), respectively and at 1530 cm^{-1} due to N-H bending vibrations (amide II). Such absorption bands were indicative of the formation of urethane linkages. The urethane and amide groups also showed an absorption band at 3347 cm^{-1}, ascribed to N-H stretching. The complete conversion of the monomers was proved by

the absence of an absorption peak at 2200 cm^{-1} due to unreacted diisocyanate.

Polyurethane average numeral molecular weight (M_n) obtained by SEC was in the 50000-55000 Da range, with a polydispersity index of 1.3. PEU low polydispersity index indicated a narrow distribution of the molecular weight.

Sol-gel transition characterization

Micelle size analysis

NHP407 and P407 solubilized in aqueous media are expected to organize into micelles with a hydrophobic core and a hydrophilic shell due to their amphiphilic properties.[23,33,34] DLS measurements were performed to study the hydrodynamic diameter of the polymeric structures formed by P407 and NHP407 solubilized in PBS as a function of solution concentration and temperature.

DLS analysis showed that unimers, micelles and aggregates were present in the solutions depending on the solubilized polymer, solution concentration and temperature.[22,35] As an example, **Figure 2** reports light scattering intensity patterns for a 1%w/v concentrated solution of P407 and NHP407 at four different temperatures (25, 30, 37 and 45 °C).

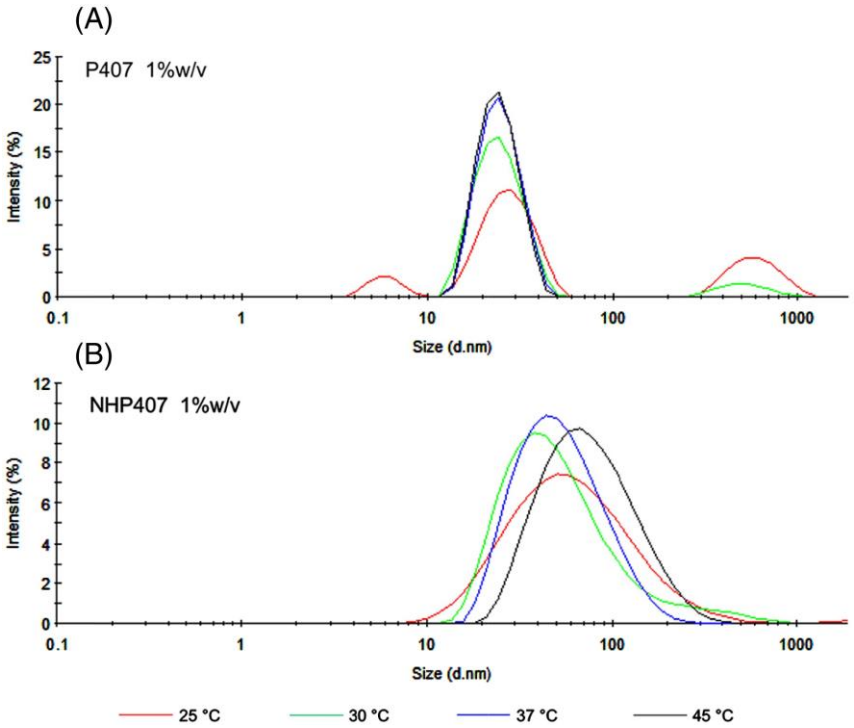

Figure 2. DLS patterns for (A) P407 and (B) NHP407 solutions with 1%w/v concentration at 25 °C (red), 30 °C (green), 37 °C (blue) and 45 °C (black). Unimers (about 6 nm diameter), micelles (about 30 nm diameter) and aggregates (about 650 nm diameter) are present in P407 sample at 25°C. With increasing temperature, unimers form micelles whereas aggregates are incorporated into the hydrophobic micelle core. On the contrary, NHP407 solution with the same concentration is already completely organized in micelles at 25°C (about 90 nm diameter).

The size distribution among unimers, micelles and aggregates was temperature-sensitive. For P407 solution with 1%w/v concentration, unimers (6.4±0.4 nm), micelles (28.2±0.3 nm) and aggregates (652.5±44.7 nm) were observed at 25°C. With increasing temperature, P407 unimers formed micelles whereas P407 aggregates were incorporated into the hydrophobic micellar core.[35] Therefore, the micellar structure became progressively prevalent with increasing temperature in P407 solution with 1%w/v concentration. Moreover, P407 micelle size has been reported to decrease with increasing the temperature, due to PEO unit dehydration.[22,35] For the P407 solution with 1%w/v concentration, the average micelle size slightly decreased from 28.2±0.3 nm at 25°C to 24.5±0.0 nm at 45°C.

On the contrary, NHP407 solution with 1%w/v concentration was already completely organized in micelles at 25°C. The average micelle diameter decreased from 88.9±10.3 nm

at 25°C to 57.3±4.0 nm at 37°C and then increased to 70.7±17.1 nm at 45°C. The different behavior between P407 and NHP407 micelles was probably due to the strong attractive inter-micellar interactions in NHP407 solution, leading to micellar clustering, dominating over PEO dehydration phenomena.[36] The presence of bridged micellar clusters or larger micelles due to aggregation phenomena was also suggested by the wide distribution of the average micelle size in the case of the NHP407 solution (1%w/v) compared to P407 solution (1% w/v) (**Figure 2**).[37]

In agreement with data reported by Cohn et al.,[18] P407 micelle size was not dependent on solution concentration: at 25°C the micelles of P407 solutions with 0.5 and 1%w/v concentrations were of 24.0±0.8 and 28.2±0.3 nm average size, respectively. On the contrary, NHP407 micelle dimension increased with increasing solution concentration: at 25°C the micelles of NHP407 solutions with 0.5 and 1%w/v concentrations were of 46.0±6.9 and 88.9±10.3 nm average size, respectively. The different behavior between NHP407 and P407 solutions with the same concentrations was probably due to aggregation phenomena of NHP407 micelles, due to the higher molecular weight of NHP407 compared to P407.

CMT evaluation

UV-Vis spectroscopy was performed on diluted NHP407 and P407 solutions at different temperatures in the presence of DHP, to measure the CMT, which is the temperature at which micellar structures start to form in the polymer solutions.

At low temperatures, NHP407 and P407 polymeric chains in solution did not arrange into micelles, as demonstrated by the negligible UV-Vis absorption at 356 nm which was indicative of the non-solubilization of DPH in a hydrophobic environment (**Figure 3A**). At increasing temperatures, UV-Vis spectrum of both NHP407 and P407 solutions showed a strong absorption at 356 nm, attributed to DHP solubilization into the hydrophobic micelle core, thus suggesting micelle formation (**Figure 3A**). In addition, the intensity of such

absorbance band increased with increasing the temperature, indicating a higher level of organization among the micelles (**Figure 3B**).

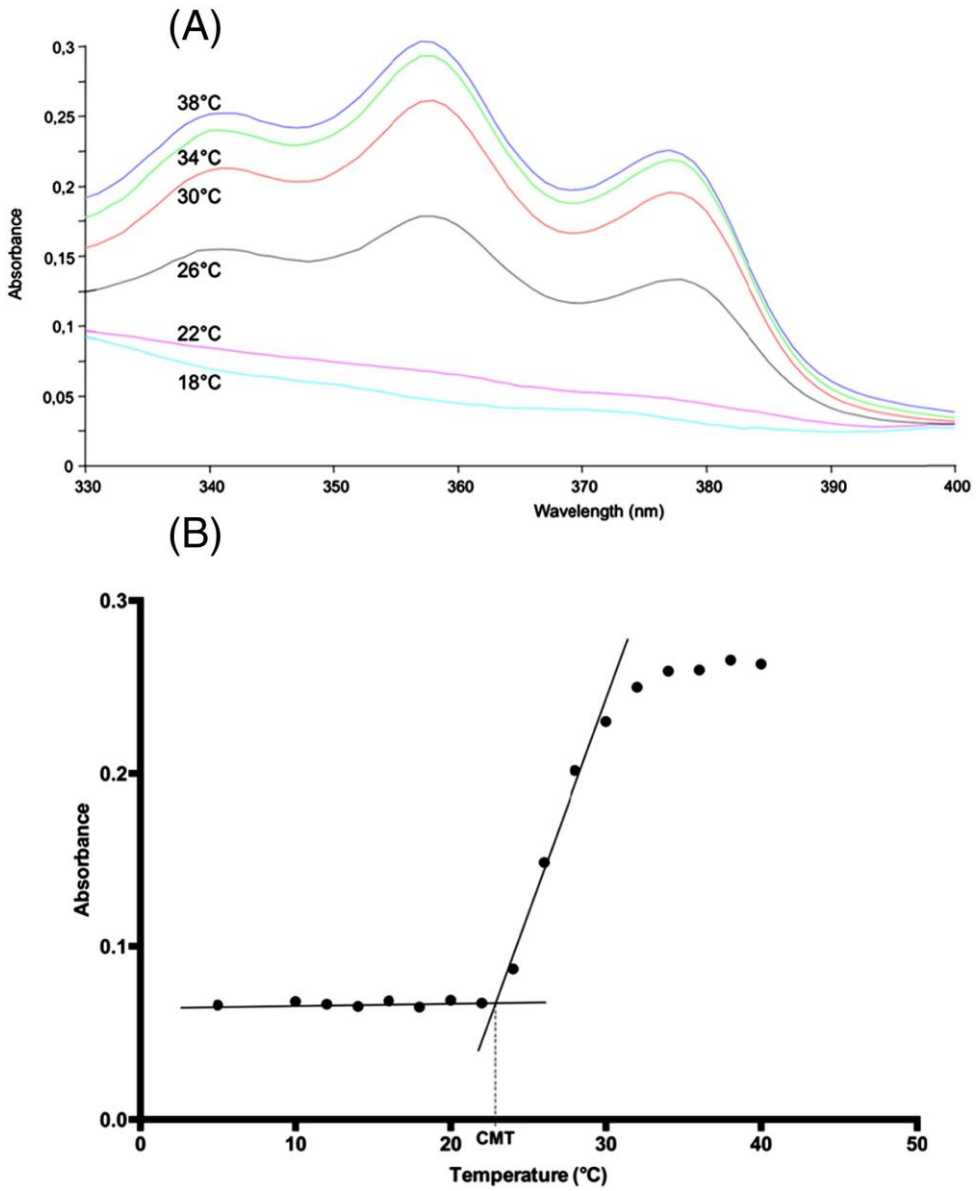

Figure 3. (**A**) UV-Vis absorption spectra of DPH/NHP407 solution (0.5%w/v) at different temperatures (18, 22, 26, 30, 34 and 38 °C). The appearance of an absorption peak at 356 nm (due to DHP solubilization into the hydrophobic micelle core) proves micelle formation. (**B**) Absorption intensity of DPH/NHP407 solution (0.5%w/v) at 356 nm as a function of temperature. CMT is estimated from the first inflection of the sigmoidal curve.

CMT of the analyzed samples was estimated from the first inflection of the sigmoidal curve of the absorption intensity at 356 nm *versus* temperature, as it was caused by the formation

of hydrophobic domains (**Figure 3B**). CMT values obtained for NHP407 and P407 solutions are listed in **Table 2** as a function of copolymer concentration.

Table 2

For both NHP407 and P407 solutions, the progressive increase of polymer concentration caused a decrease of CMT. At the same polymer concentration, NHP407-based solutions showed a slightly lower CMT than P407-based ones (of around 1-2°C) (not-significant difference).

Phase diagram and gelation time at physiological conditions

Figure 4 reports the phase diagrams for P407- and NHP407-based solutions in PBS, while the values of sol-gel transition (LCGT) and gel-sol transition (UCGT) temperatures are reported in **Table 3.**

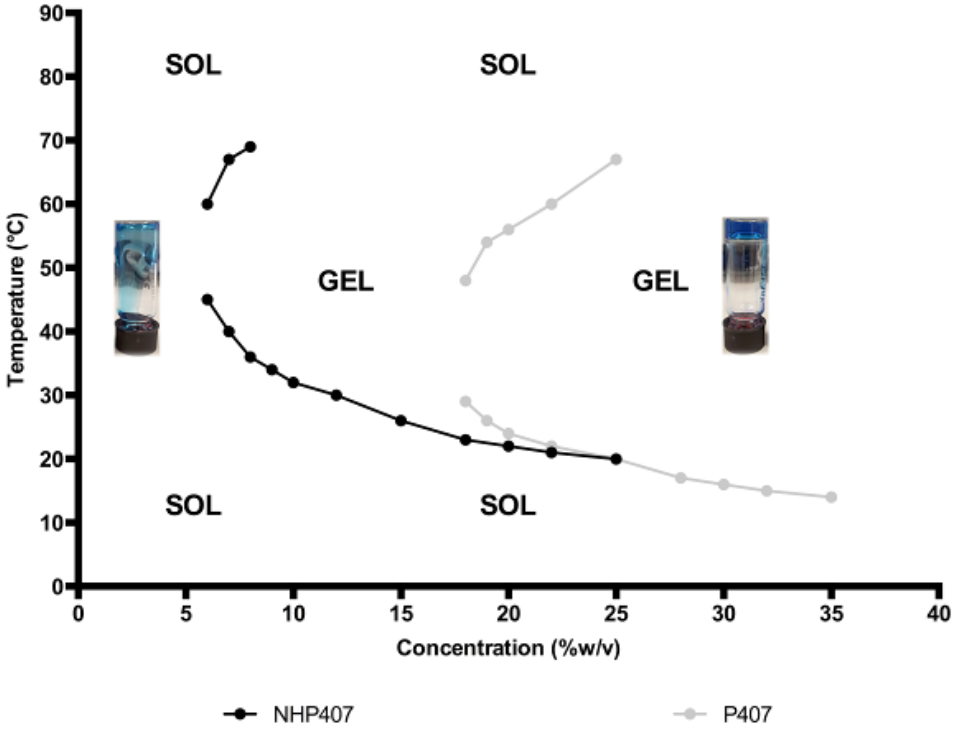

Figure 4. Sol-gel-sol transition curves for P407- (grey) and NHP407-based (black) solutions in PBS obtained by tube inverting test. Sol and gel regions are indicated and properly imaged with photos of two samples. Conditions of sol and gel were defined as “flow liquid sol” and “no flow solid gel” within 30s, respectively. NHP407 solutions exhibit different sol-gel-sol transition behavior compared to P407- solutions, with a lower critical gelation concentration (CGC).

Table 3

NHP407 solutions exhibited different sol-gel transition behavior compared to P407- solutions, with a lower CGC value of 6±1%w/v respect to 18±1%w/v for P407 solutions.[38,39] In addition, T**able 3** showed that at the same solution concentration (18-25%w/v), LCGT values for NHP407 solutions were generally lower than for P407 solutions. However, the differences in LCGT decreased with increasing solution concentration.

Tube inverting test was also performed on NHP407 and P407 solutions prepared in DMEM (data not reported) to analyze the influence of the solvent type on CGC, LCGT and UCGT values. However, no significant differences were observed. Therefore, although DMEM and PBS composition is different, their overall effect of on phase transitions of P407 and NHP407 systems was approximately the same.[40]

Finally, the gelation time at 37°C of the P407 and NHP407 solutions in PBS was studied as a fundamental parameter for the use of the hydrogels as injectable systems (**Figure 5**). For NHP407 solutions, gelation time decreased with increasing solution concentration from 15-30 min at 6%w/v concentration to within 5 min at 10-25% w/v concentration. A similar behavior was observed for P407 solutions which gelation time decreased from 15-30 min at 18%w/v concentration to within 5 min at 20-25%w/v concentration. When comparing the two materials, solutions with 18%w/v concentration gelled at 37°C after 15-30 min in the case of P407 and within 5 min for NHP407. On the other hand, P407 and NHP407 solutions with 20-25%w/v concentration both gelled within 5 min at 37°C.

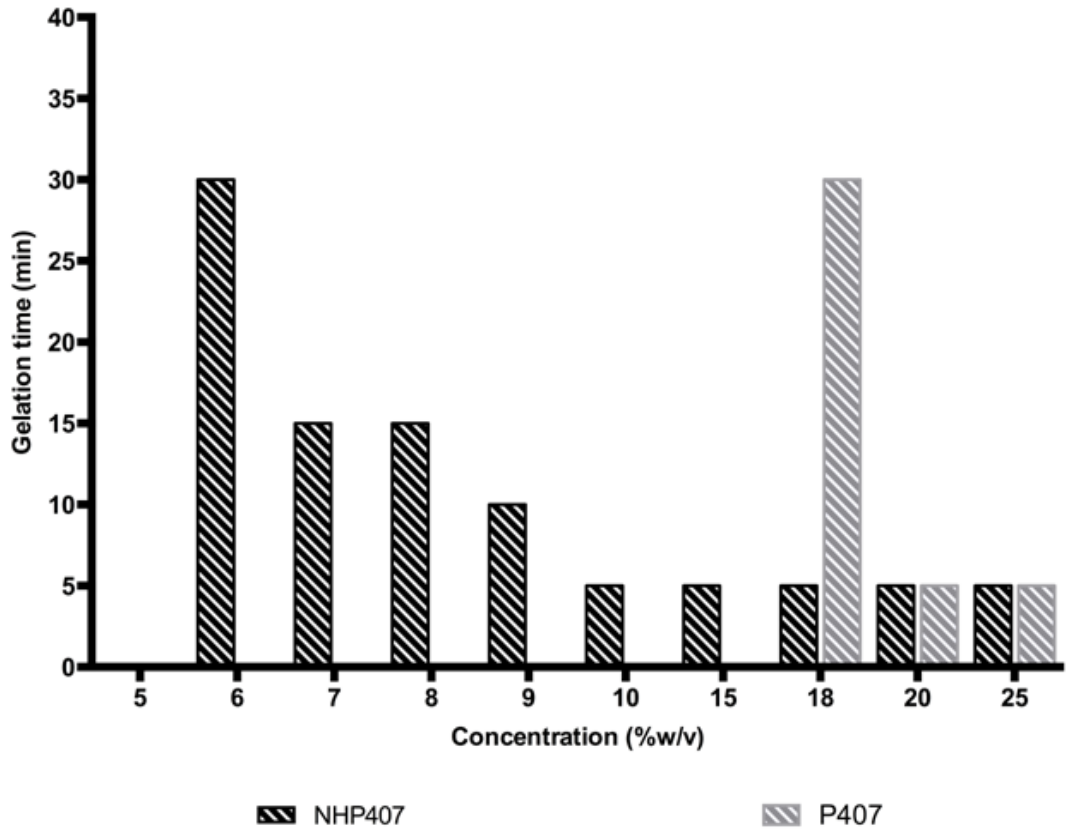

Figure 5. Gelation time at 37°C of P407 (gray) and NHP407 (black) solutions. For both the analyzed polymers, gelation time decreases with increasing solution concentration, and NHP407-based solutions show a faster gelation that P407-based ones with the same concentration (for 20 and 25 %w/v concentrated solutions no differences were observed since both samples were completely gelled at the first analyzed time, i.e. 5 minutes).

Rheological characterization

The sol-gel transition of NHP407 and P407 solutions was also analyzed by rheological characterization by temperature ramp tests at constant shear (10 s^{-1}) and 1°C/min heating rate.

The behavior of viscosity as a function of temperature during the sol-to-gel transition of NHP407 systems with different concentration is reported in **Figure 6A.**

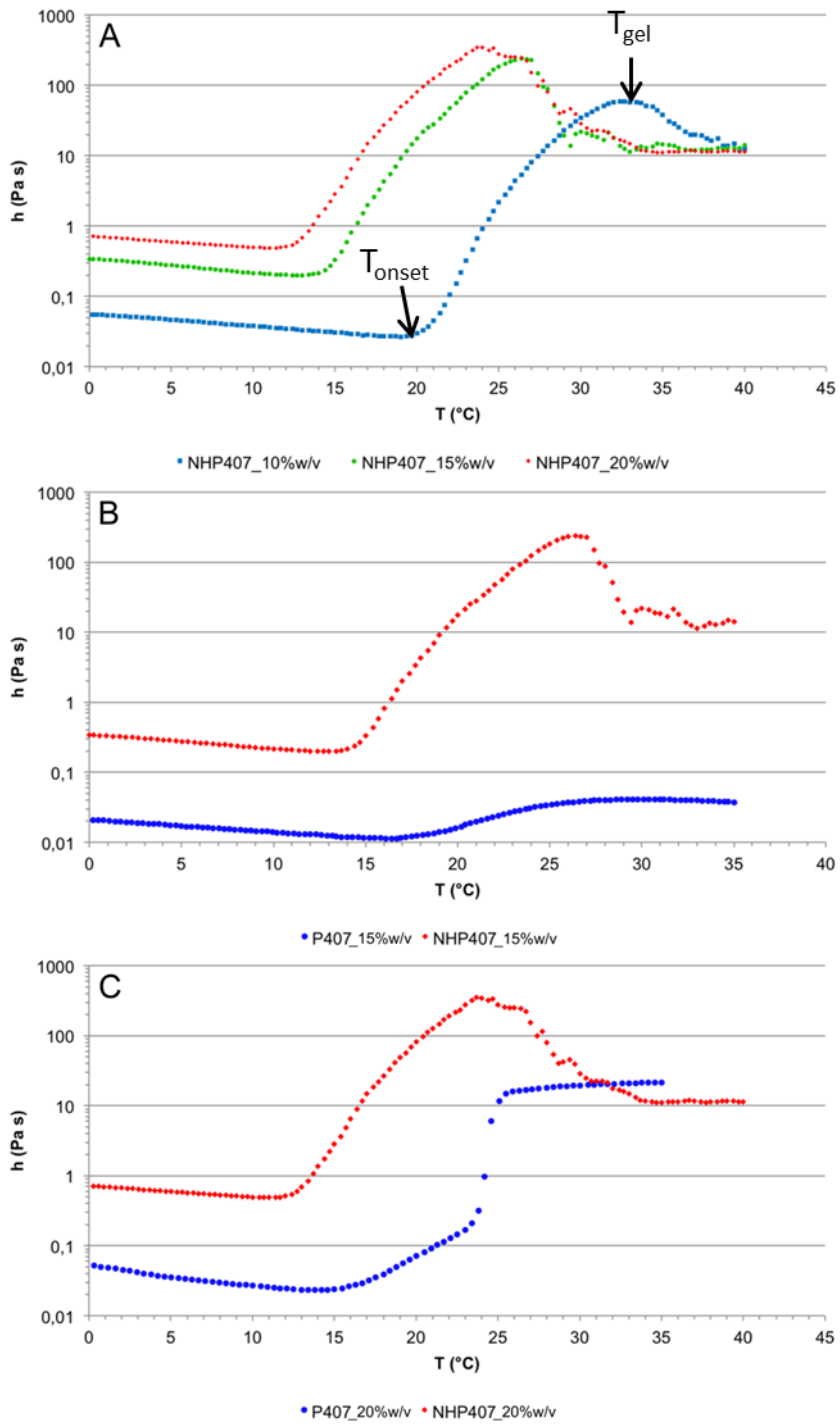

Figure 6. Viscosity (h) versus temperature (T) during sol-to-gel transition as analyzed by temperature ramp test. (**A**) NHP407 systems at 10 (blue), 15 (green) and 20%w/v (red) concentrations. Gelation onset temperature (T_{onset}) and gelation temperature are defined at the minimum value of sol viscosity and at 95% viscosity maximum value, respectively. (**B**) and (**C**) comparison between NHP407 (red) and the corresponding P407 (blue), with 15% w/v (B) and 20%w/v (C) concentrations. For all the analyzed samples, viscosity decreased as a function of temperature, as it is typical of a sol phase; after a minimum value of viscosity is reached, viscosity starts to monotonically increase as a consequence of micelle nucleation. After complete gelation, the viscosity of the NHP407 system decreased with increasing temperature, due to a melt fracture phenomenon. P407-based gels are weaker than NHP407 gels having the same concentration.

Initially, the viscosity decreased as a function of the temperature, as it is typical of fluid systems (sol phase). A minimum value of viscosity was reached, followed by a monotonic increase in viscosity, due to micelle nucleation. Then, viscosity sharply increased as a function of temperature during the growth of micelles with the conversion of the homogeneous fluid into a biphasic system. Finally, viscosity reached a maximum value and the gelation process was completed.

Two characteristic temperatures could be defined from such curves (**Figure 6A**):

- the gelation onset temperature (T_{onset}), at the minimum value of sol viscosity;
- the gelation temperature (T_{gel}), at 95% viscosity maximum value.

After complete gelation, the viscosity of the NHP407 system decreased with increasing the temperature, differently from P407 hydrogel with the same concentration, which viscosity remained constant (**Figure 6B** and **6C**). This effect was not due to some transition within the material, but rather to melt fracture of the system, i.e. the gel, subjected to a continuous strain rate, slided out of the plates and crumbled.

P407 solutions with 10%w/v (not shown) and 15%w/v (**Figure 6B**) concentration did not form a gel-phase at the conditions of the temperature ramp test. On the contrary, P407 solution with 20%w/v concentration converted into a gel with increasing the temperature (**Figure 6C**), although the formed gel was weaker than the NHP407 gel having the same concentration. A comparison between the results from the tube inverting tests and rheological analysis is reported in **Table 4**. Data deriving from both characterizations were in good agreement: some small differences were probably due to the different analysis conditions, as the tube inverting test does not apply deformations while the temperature ramp test is performed under constant deformation.

Table 4

Strain sweep tests displayed the typical response of an associative polymer structure, as illustrated in **Figure 7**, which reports the behavior of G'/G'$_0$ and G''/G''$_0$ as a function of the strain (γ) for NHP407 hydrogels. On the other hand, **Figure 8** shows the behavior of G' and G'' as a function of the strain for NHP407 and P407 hydrogels with the same concentration (20%w/v). With increasing γ above a critical value, G' started to decrease; on the contrary, G'' initially increased and, then, decreased suggesting an overshoot phenomenon (i.e. a strain hardening effect).

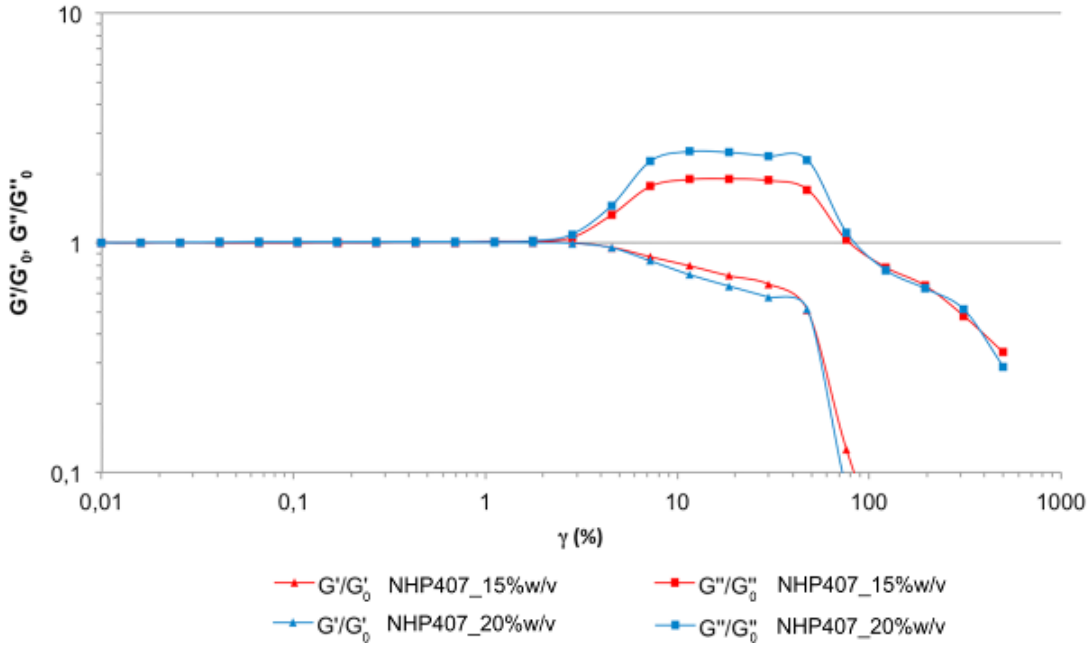

Figure 7. Behavior of G'/G'$_0$ and G''/G''$_0$ as a function of the applied strain (γ) for NHP407 hydrogels with 15 and 20%w/v concentrations at 37°C. G' and G'' are the storage and loss moduli, respectively, while G'$_0$ and G''$_0$ are their initial plateau values. Both the analyzed samples displayed the typical response of an associative polymer structure.

YS and G'' peak intensity increased with increasing NHP407 concentration in PBS, whereas the strain at G'' maximum was approximately unchanged (**Table 5**). Probably, the effect of NHP407 hydrogel concentration on the gel-phase rheological properties was mainly due to a higher amount of micelles, rather than to a change in micelle morphology.

Table 5

Although both NHP407 and P407 hydrogels showed the typical behavior of structured systems (evidencing strain hardening effect), the resistance to deformation of NHP407 hydrogels (i.e. the strain at G'' peak and the YS value) was higher than for the corresponding P407-based hydrogels (**Figure 8** and **Table 5**).

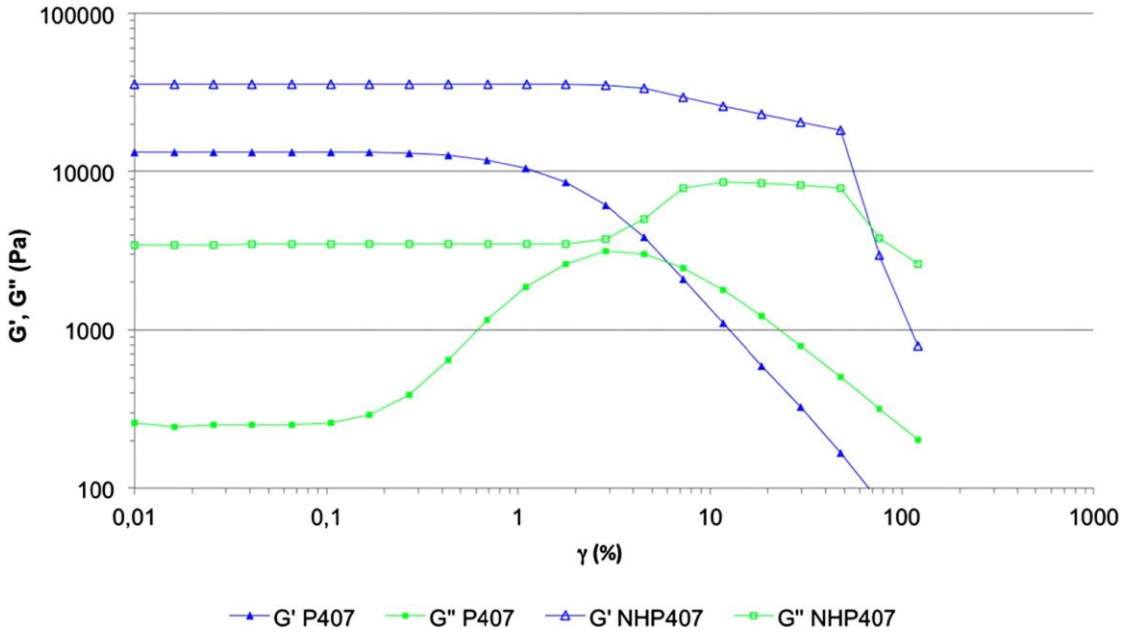

Figure 8. Elastic (G') and viscous (G'') moduli versus strain (γ) for NHP407 and P407 with 20%w/v concentration at 37°C. Although both NHP407 and P407 hydrogels exhibit the behavior of structured systems (i.e. strain hardening effect), NHP407 hydrogels show higher resistance to deformation (i.e. strain at G'' peak) than P407-based hydrogels with the same concentration.

Fully-developed hydrogels are known to be monophasic with G' values independent on frequency. The viscoelasticity of NHP407 hydrogels at different temperatures is reported in **Figure 9**, **10A** and **10B**. The elastic modulus (G') of NHP407 hydrogel with 10%w/v concentration at 37°C (**Figure 9**) was frequency-dependent at low frequencies, as it is characteristic of a fluid system. Hence a temperature of 50°C was required to obtain a fully

developed hydrogel (the elastic modulus was independent on frequency only at temperatures ≥ 50°C).

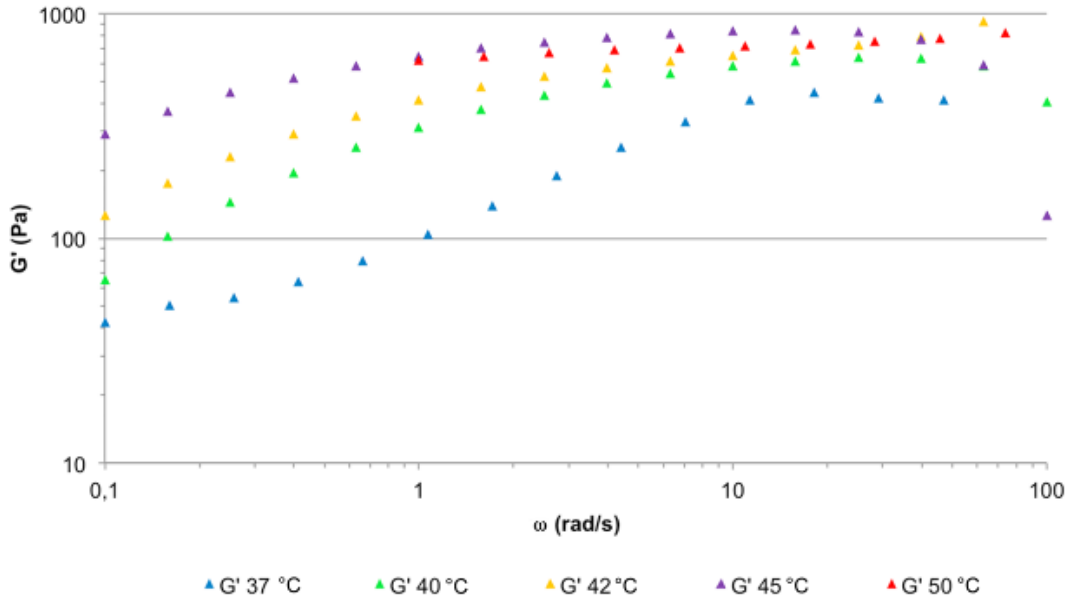

Figure 9. Storage modulus (G') as a function of frequency (ω) at different temperatures (37, 40, 42, 45 and 50 °C) for NHP407 hydrogel with 10%w/v concentration (γ=0.1%). At 37 °C, G' is frequency-dependent at low frequencies, as it is typical of a fluid system. A temperature of 50 °C is required to make the analyzed sample a fully developed hydrogel (i.e. G' independent on frequency).

For higher concentrated hydrogels, **Figure 10A** shows that G' was approximately constant even at low frequencies. However, NHP407 system with 15%w/v concentration was not a fully-developed hydrogel at 37°C, and gelation was complete only at a temperature ≥ 40°C. On the contrary, NHP407 system with 20%w/v concentration was already a fully developed hydrogel at 37°C. As soon as the fully-developed hydrogel conditions were reached, the effect of a further increase in temperature on the viscoelastic behavior was negligible; on the contrary, any increase of NHP407 concentration strongly affected elastic modulus (G' of NHP407 hydrogel with 20%w/v concentration was about twice that of NHP407 hydrogel with 15%w/v concentration).

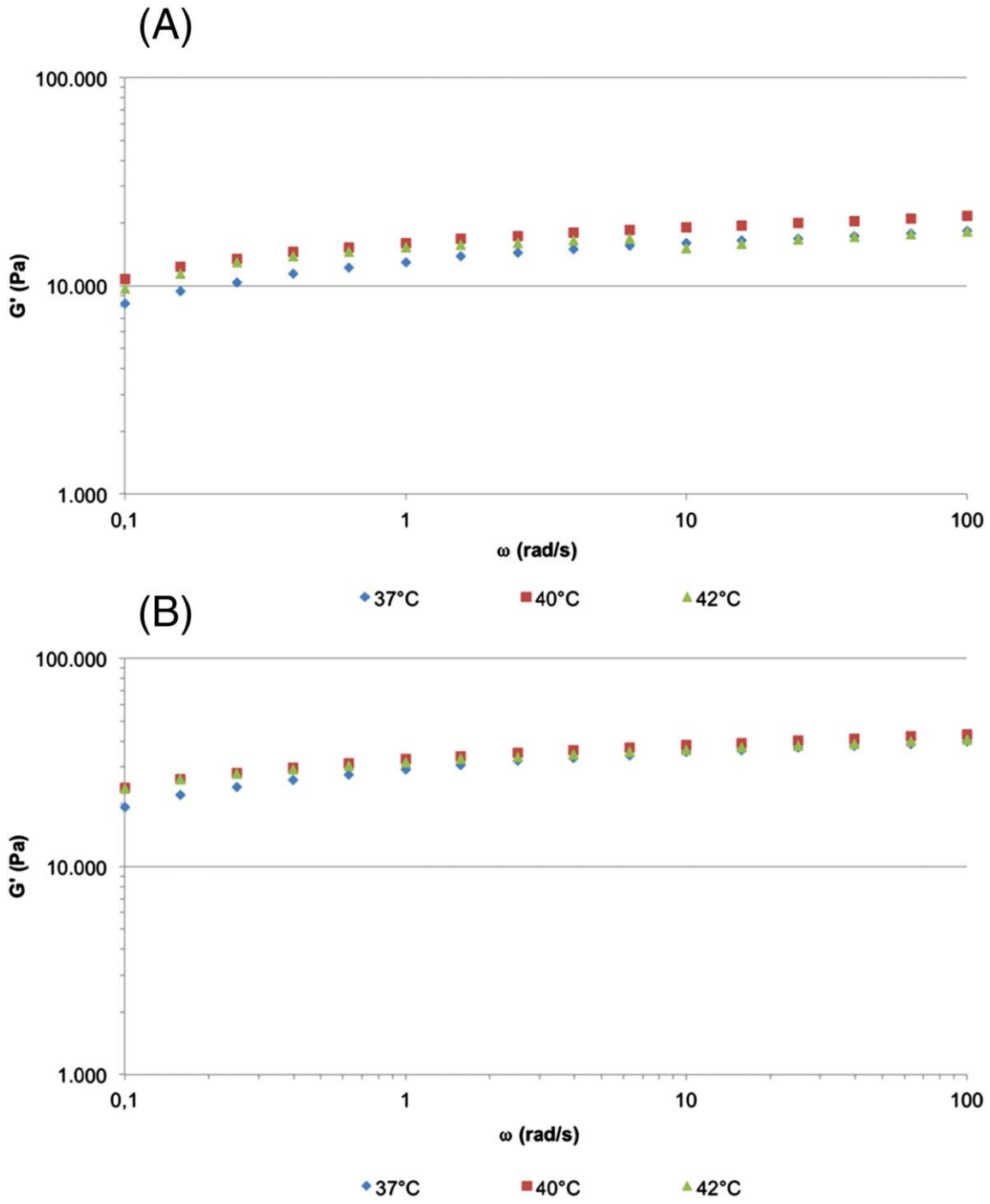

Figure 10. Elastic modulus (G') versus frequency (ω) at different temperatures (37, 40 and 42 °C): (**A**) NHP407 hydrogel with 15%w/v concentration, (**B**) NHP407 hydrogel with 20%w/v concentration. NHP407 system with 15%w/v concentration is not a fully-developed hydrogel at 37°C, and gelation is complete at temperature ≥ 40°C. On the contrary, NHP407 system with 20%w/v concentration is already a fully developed hydrogel at 37°C. After the achievement of fully-developed hydrogel conditions, a further increase in temperature does not significantly influence the viscoelastic behavior of the formed gel.

The G' independent behavior on frequency suggested that the chains have to disentangle before undergoing relaxation in response to stresses. The disentanglement process is

related to the length scale of the entanglement spacing (a) and the (average) monomer size (b) through the Doi and Edwards equation.[41]

The domain entanglement spacing for NHP407 hydrogels at different temperatures are reported in **Table 6**.

Table 6

Results confirmed the compact structure of PEU hydrogels and its dependence on temperature. As the monomer size (b) was constant, the entanglement spacing increased as a function of temperature. The entanglement spacing of NHP407 hydrogel with 10%w/v concentration was large, confirming the bi-phasic nature of this system.

Gel stability and degradation

Stability tests of P407 and NHP407 hydrogels with 20%w/v concentration were performed in PBS at 37°C as a function of time, evaluating the change in weight, which is indicative of swelling or dissolution phenomena (**Figure 11**).

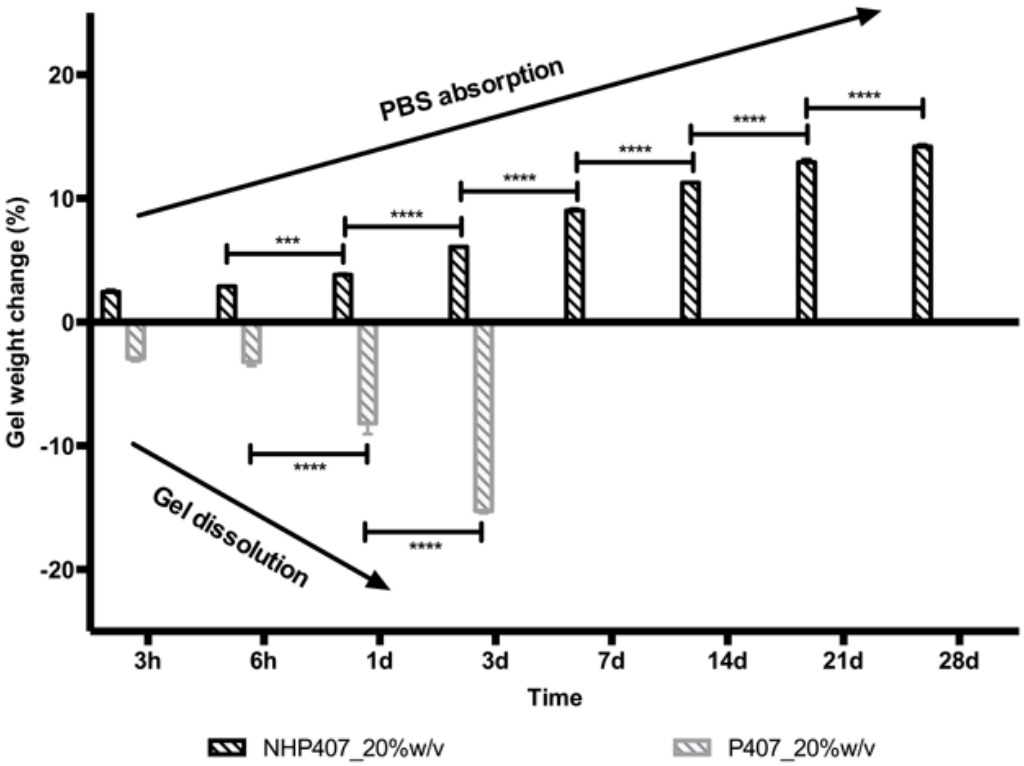

Figure 11. Gel weight change (%) as a function of time for P407 and NHP407 hydrogels with 20%w/v concentration. NHP407-based gel progressively increases its weight as a function of time because of PBS absorption, while P407 hydrogel with the same concentration progressively loses its weight and completely dissolves after 5 d.

NHP407 hydrogel with 20%w/v concentration progressively increased its weight as a function of time probably due to PBS absorption. On the contrary, P407 hydrogel progressively lost its weight with increasing incubation time and completely dissolved after 5 d. In addition, HP407 hydrogels with 10, 15 and 20%w/v concentrations were characterized in terms of PBS absorption (**Figure12A**) and PEU dissolution (**Figure 12B**) as a function of time, according to Eq. 1 and 2, respectively.

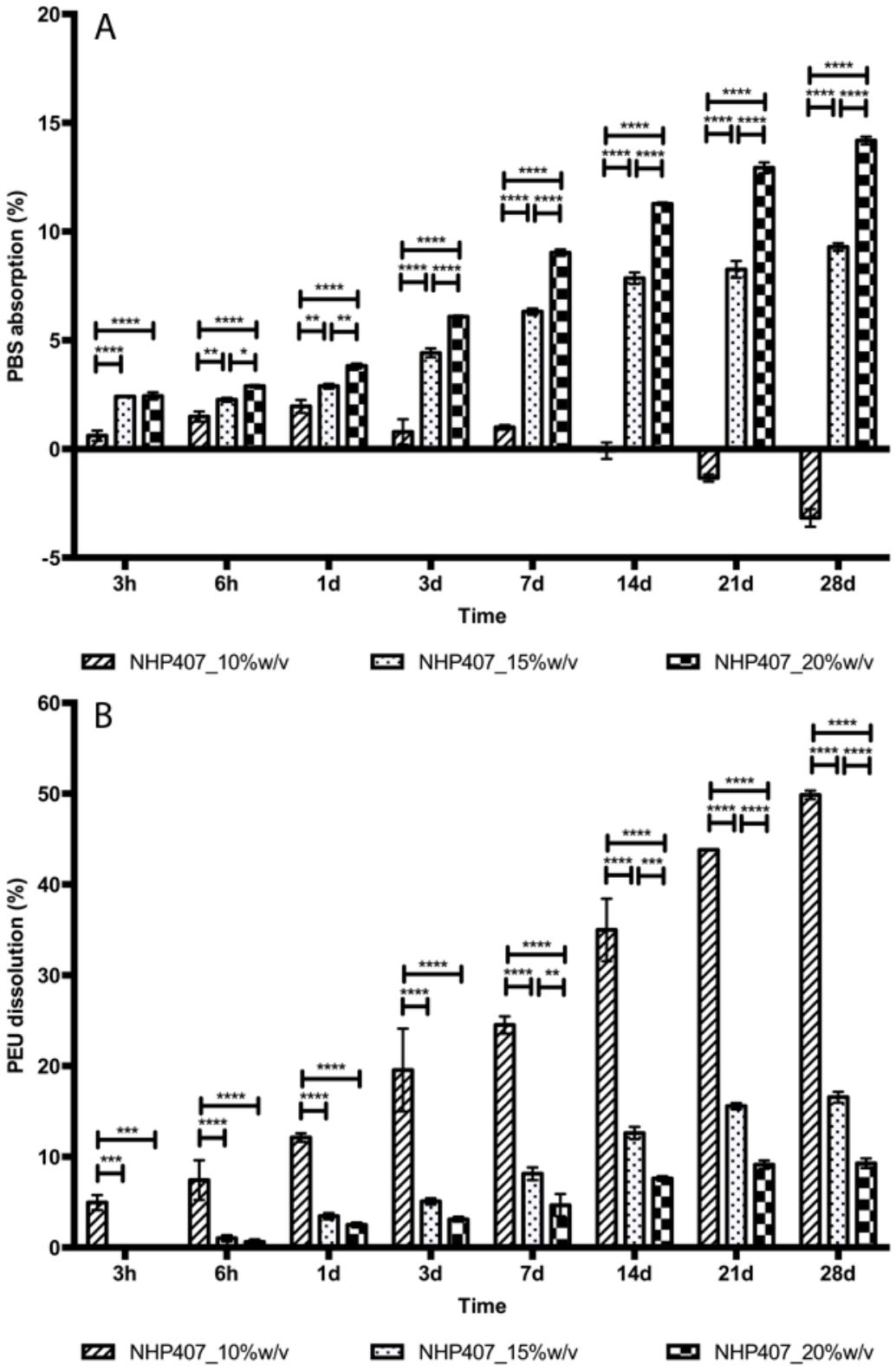

Figure 12. NHP407 hydrogels with 10, 15 and 20%w/v concentrations: PBS absorption (A) and PEU dissolution (B) as a function of time. PBS absorption increases as a function of time for NHP407 hydrogels with 15 and 20%w/v concentrations, while for NHP407 hydrogel with 10%w/v concentration the appearance of a negative change in weight suggests a partial hydrogel dissolution. PEU dissolution degree increases as a function of time for all the analyzed hydrogels and it is more pronounced for the less concentrated hydrogels at each time interval.

For NHP407 hydrogels with 15 and 20%w/v concentrations, PBS absorption (**Figure 12A**) increased as a function of time; at each analyzed time interval, PBS absorption was the highest for the 20%w/v concentrated hydrogel compared to the other two concentrations. On the other hand, NHP407 hydrogel with 10%w/v concentration showed a limited PBS absorption up to 7 days and, after 21-25 days, showed a negative change in weight, suggesting partial dissolution.

Dissolution degree (**Figure 12B**) increased as a function of time for all the hydrogels and it was more pronounced for the less concentrated hydrogels at each time interval. Dissolution level of the 10%w/v concentrated NHP407 hydrogel was particularly pronounced, reaching 50% after 25 days incubation in PBS at 37°C.

Permeability to nutrients

Permeability to FD4 was studied to model nutrient transport within the hydrogel.[27] **Figure 13** reports FD4 absorption as a function of time for all the analyzed NHP407 hydrogels with 10, 15 and 20%w/v concentrations. The percentage amount of absorbed FD4 increased with increasing time and, at the same time, was significantly higher for less concentrated hydrogels.

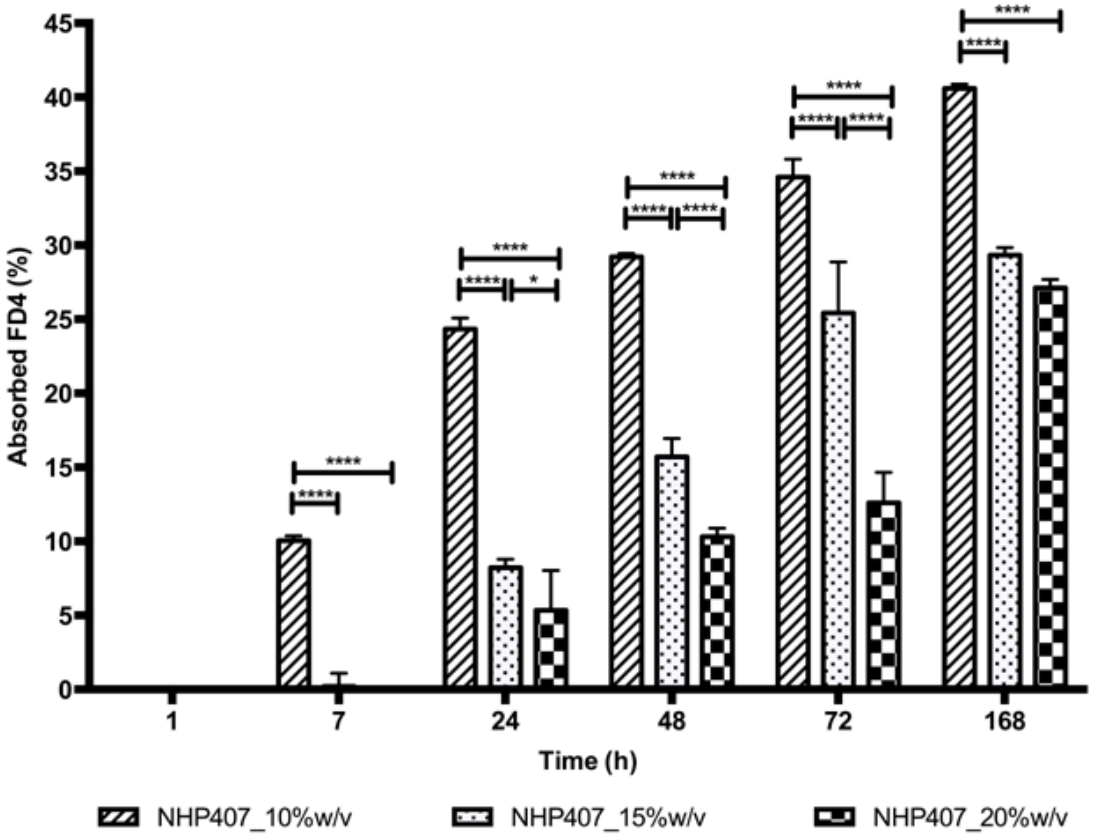

Figure 13. Percentage amount of FD4 (model of nutrients) absorbed by NHP407 hydrogels with 10, 15 and 20%w/v concentrations as a function of time. The amount of absorbed FD4 increases with increasing time and, at the same time, is significantly higher for less concentrated hydrogels.

Qualitative evaluation of hydrogel injectability

Injectability of NHP407 solutions and hydrogels with 10, 15 and 20%w/v concentrations was evaluated using syringes with needles of 0.20 and 0.25 mm internal diameter. At 5°C, all the systems were in sol phase and easily injectable. At 25°C, mixed sol-gel phases were present and again the material was injectable at each tested condition. At 37°C, NHP407 hydrogels formed and they could be injected at each tested condition, with the exception of the hydrogel with 20%w/v concentration that turned out injectable only through the syringe with 0.25 mm needle size.

To qualitatively evaluate the shape stability of the formed hydrogel at 37°C, P407 and NHP407 solutions with 10, 15 and 20%w/v concentrations were prepared at 5°C and, then, injected into a water bath kept at 37°C. **Figure 14** shows the results for the hydrogels with

20%w/v concentration: the NHP407 hydrogel rapidly formed after injection and assumed a fibrous shape, while the P407 hydrogel showed the tendency to rapidly dissolve in contact with the water medium, as suggested by the light blue color assumed by the water bath.

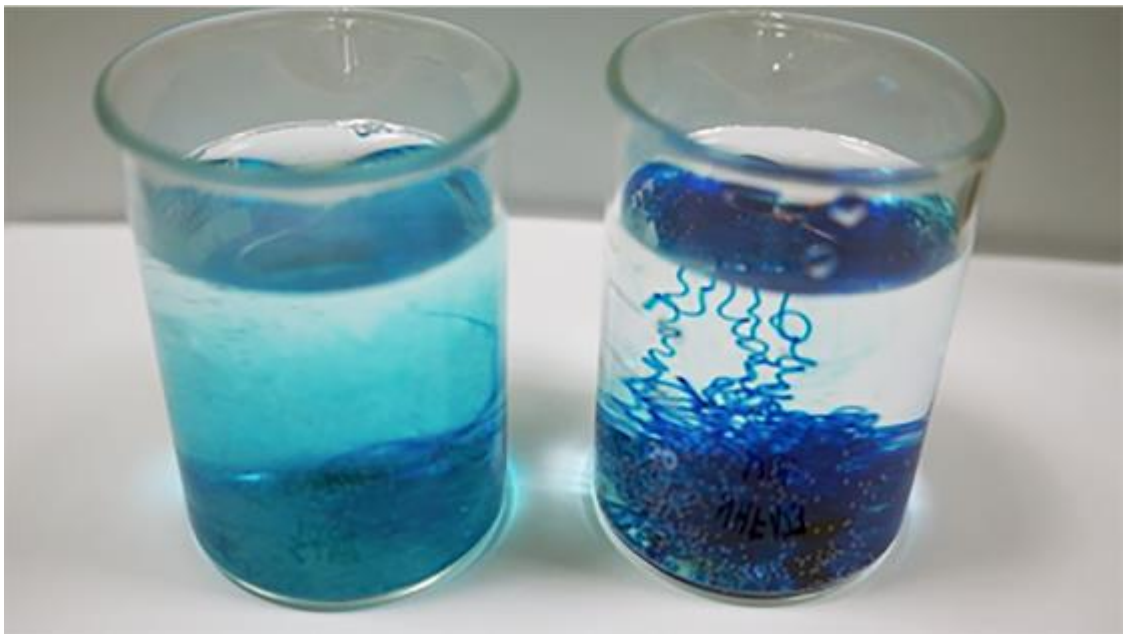

Figure 14. Image of injected P407 (left) and NHP407 (right) solutions with 20%w/v concentration (prepared and conditioned at 5°C) in a water bath kept at 37 °C. NHP407 hydrogel rapidly forms after injection and assumes a fibrous shape, while P407 hydrogel with the same concentration shows the tendency to rapidly dissolve in contact with water.

NHP407 systems with 10 and 15%w/v concentrations showed a similar behavior to P407 and NHP407 solutions with 20%w/v concentrations, respectively.

Cytotoxicity tests

Preliminary cytotoxicity tests were carried out using keratinocytes HaCaT, C_2C_{12} muscle cells and human fibroblast (46 BR.1N) to assess the biocompatibility of the newly synthesized NHP407 hydrogel. In the case of keratinocytes, NHP407 hydrogel with 20%w/v concentration showed a significantly lower cytotoxicity respect to P407 hydrogel with the same concentration (cell viability respect to the control: 83±10% and 51±9%, respectively), while, for C_2C_{12} muscle cells and fibroblasts, P407 hydrogels showed a higher level of

biocompatibility with respect to NHP1407 hydrogels with the same concentration (cell viability respect to the control: 146±3% and 104±15% for fibroblasts, respectively, and 117±14% and 104±8% for C_2C_{12} muscle cells, respectively).

Discussion

In this work, a novel amphiphilic poly(ether urethane) (NHP407), was successfully synthesized as assessed by SEC and ATR-FTIR analysis (**Figure 1**), soluble in water-based media at defined temperature conditions and undergoing a thermo-responsive gelation. The objective of the work was to design a new polymeric material with improved gelation ability, mechanical strength and stability in physiological environment with respect to a commercially available FDA-approved Poloxamer, Poloxamer P407. The phase diagram of P407- and NHP407-based solutions in PBS was obtained by the tube inverting test (**Figure 4**). Both systems showed a LCGT behavior. The significantly lower CGC of NHP407 hydrogels (6%w/v) with respect to P407-based ones (18%w/v) could be attributed to the larger micelles formed by NHP407 solubilized in aqueous media, as demonstrated by DLS analysis performed on diluted solutions (**Figure 2**). The larger micelles of NHP407 solutions reached the critical volume of 0.53 (the value required for reverse thermal gelation) at lower solution concentration than for P407 systems.[42,43] In addition, at the same concentration, NHP407-based solutions exhibited a slightly lower CMT than P407-based ones (of about 1-2°C) (**Table 2**), which suggested a higher micellization rate.[37]

Results from the tube inverting test and rheological temperature ramp analysis (**Figure 4** and **6**) were in good agreement, demonstrating that the tube inverting test is a valuable tool for a preliminary determination of the sol-gel-sol transition of thermosensitive hydrogels. The shift of NHP407 sol-to-gel transition curve to lower concentrations as well as the lower CMT at the same solution concentration was found to be influenced by several factors. The dependence on many other parameters than the sole molecular weight was suggested by

the fact that at the same solution molarity, P407- and NHP407-based solutions convert into gels at very different temperatures (at 2 mM concentration, P407-based solution does not gel, while NHP407 sample undergoes a sol-to-gel transition at 32°C). Therefore, several mechanisms probably accounted for the significantly different gelling behavior of NHP407 compared to P407 solutions such as: (i) the formation of higher hydrophobic interactions and bridges between the micelles due to NHP407 longer chains, (ii) micelle clustering, as confirmed by DLS measurements, (iii) hydrogen bonding between the micelles due to NHP407 urethane groups and (iv) the achievement of the critical volume required for gelation at lower solution concentrations, as a consequence of NHP407 larger micelles/micelle aggregates.[42,43] Therefore, the different trend of viscosity *versus* temperature between P407 and NHP407 systems with 20%w/v concentration (**Figure 6C**) could be ascribed to a different gelation mechanism: P407 system underwent a two-step gelation, while NHP407 solution became a gel through a one-step mechanism, that probably resulted from different kinetics in micelle formation, as shown by DLS measurements for P407 and NHP407 solutions. This hypothesis was also confirmed by the different consistence and rheological properties of the resulting hydrogels: while P407 gels showed a creamy-like appearance, NHP407 gels exhibited a compact and solid-like structure (**Figure 15**) and were characterized by higher G', G'', YS and γ_{max} than P407 hydrogels with the same concentration.

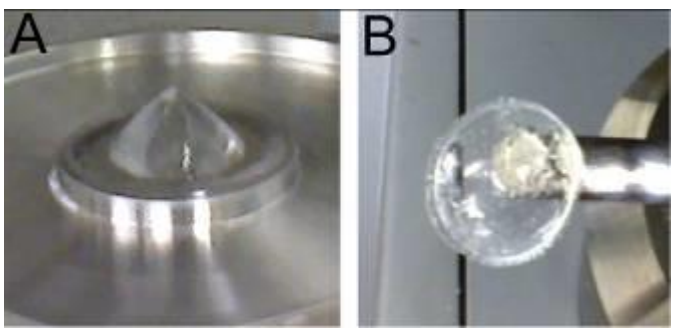

Figure 15. Gel structure after frequency sweep test at 37°C. P407 (**A**) and NHP407 **(B)** hydrogels with 20%w/v concentration. While P407 gel shows a creamy-like appearance, NHP407 gel with the same concentration exhibits a compact and solid-like structure.

NHP407-based solutions showed a faster gelation than P407-based ones and the formed gels were stable in a wider temperature range as demonstrated by the phase diagram (**Figure 4**). Moreover, whereas P407 hydrogel with 20%w/v concentration rapidly dissolved within 5 days, NHP407 hydrogel with 20%w/v concentration was stable in aqueous media up to 28 days (**Figure 11**).

A suitable hydrogel for application as in situ cell and/or drug carrier should exhibit (i) a fast gelation in physiological conditions, (ii) an easy injectability in the sol state followed by gelation at 37°C, thus allowing the complete filling of body cavities and defects before gelation, (iii) a suitable composition to allow fast nutrient and oxygen supply to the encapsulated cells as well as waste removal, and (iv) tunable residence time, achievable by changing hydrogel composition, to modulate cell and/or drug release. In addition, hydrogels are commonly exploited as scaffold-forming materials in bioprinting technologies, that fabricate layer-by-layer 3D constructs according to a computer-aided draft.[44–46] Hydrogels for cell printing applications should meet further requirements in addition to the previously listed ones: (i) fast enough gelation to avoid cell sedimentation inside the hydrogel structure, (ii) injectability under low shear stresses not to affect cell viability, and (iii) capability to keep their shape in aqueous environment at 37°C for the required time. Rheological frequency sweep tests at 37°C showed that the NHP407 hydrogel with 10%w/v concentration had a liquid like behavior, while the NHP407 hydrogels with 15%w/v and 20%w/v concentrations were biphasic (as a small amount of sol was present) and complete gel, respectively (**Figure 9 and 10**). Based on these data, together with results from gelation time (**Figure 5**) and tube inverting tests (**Figure 4**), these three compositions were selected as the most promising ones for application in tissue engineering and drug release. All the characterized hydrogels, in fact, satisfied the above listed requirements for applications as cell/drug delivery injectable carriers. In addition, NHP407 hydrogels with 15%w/v and 20%w/v

concentrations demonstrated their potential applicability in bio-printing technology **(Figure 14 and 15).** NHP407 hydrogels showed permeability to the FD4 model molecule, and, as expected, the biphasic nature and lower concentration of the NHP407 hydrogels with respectively 10 and 15%w/v concentrations caused their higher permeability to FD4 respect to NHP407 hydrogel with 20%w/v concentration (**Figure 9 and 10**). A concentration-dependent dissolution kinetics was observed, with a significantly faster dissolution for the NHP407 hydrogel with 10%w/v concentration respect to the hydrogels with 20 and 15%w/v concentrations. **Figure 12A** showed that unexpectedly the NHP407 hydrogels were able to absorb an increased amount of PBS with increasing polymer concentration. This result was correlated with the data reported in **Figure 12B**, that showed a significantly faster dissolution rate of NHP407 hydrogels with decreasing concentration. Hence, hydrogels with lower concentrations absorbed a lower PBS amount due to their faster dissolution rate.

Finally, results of cytotoxicity tests performed on hydrogel extracts in contact with HaCaT keratinocyte cells, C_2C_{12} muscle cells and fibroblasts demonstrated no cytotoxicity (cell viability >80%), confirming that NHP407 hydrogels (with concentration lower or equal to 20%w/v) are promising materials for regenerative medicine applications.

Table 7 summarizes the main achievements of this work, highlighting NHP407 hydrogel advantages over Poloxamer P407-based ones.

Table 7

Conclusion

In this work, a novel reverse thermo-responsive polymeric system was successfully developed by chain extending Poloxamer P407 with an aliphatic non-toxic diisocyanate and an amino acid derived diol with Boc-protected amino groups available for further functionalization upon deprotection in acidic conditions.[20] NHP407 hydrogel overcame some

of the Poloxamer gel drawbacks, as summarized in **Table 7**. In addition, the hydrogels with a NHP407 concentration of 15 and 20%w/v showed promising properties for application in tissue engineering/regenerative medicine and drug release as *in situ* injectable cell/protein/drug delivery systems. These hydrogels, in fact, (i) underwent fast gelation in physiological conditions (a volume of 1 mL converted into a gel within 5 min incubation at 37°C), (ii) allowed nutrient and oxygen supply and waste removal, thus allowing cell encapsulation, (iii) were injectable in the form of sol, sol-gel and gel, at different temperatures and flow rates, (iv) could potentially allow prolonged drug release due to hydrogel long term stability in water media at 37°C (release kinetics could be modulated varying the hydrogel concentration as it affects permeability, as also reported by Niu at al. and Cohn et al.,[15,18]) and (v) showed a concentration-dependent dissolution kinetics. Furthermore, under certain conditions of temperature and flow rate, the NHP407 hydrogels with 15 and 20%w/v concentration showed the ability to be extruded into continuous filaments that make them potential candidates for application as scaffold-forming materials in bioprinting technologies.

Acknowledgements

FIRB 2010 Project 'Bioartificial materials and biomimetic scaffolds for a stem cells-based therapy for myocardial regeneration' (grant no. RBFR10L0GK) financed by MIUR (Italian Ministry of Education University and Research) and "Smart Injectable Drug-Delivery systems for Parkinson's and Alzheimer's Disease Treatment (PAD-INJ)" project (call for joint Projects of Internationalization of research financed by Compagnia San Paolo) are acknowledged.

References

1. Kaji H, Camci-Unal G, Langer R and Khademhosseini A, *Biochim Biophys Acta* **1810:** 239–250 (2011).

2. DeForest CA and Anseth KS, *Annu Rev Chem Biomol Eng* **3:** 421–444 (2012).

3. Camci-Unal G, Cuttica D, Annabi N, Demarchi D and Khademhosseini A, *Biomacromolecules* **14:** 1085–1092 (2013).

4. Hoffman AS, *Recent Dev Hydrogels* **54:** 3–12 (2002).

5. Peppas NA, Bures P, Leobandung W and Ichikawa H, *Eur J Pharm Biopharm* **50**: 27–46 (2000).

6. Slaughter BV, Khurshid SS, Fisher OZ, Khademhosseini A and Peppas NA, *Adv Mater* **21:** 3307–3329 (2009).

7. Vashist A, Vashist A, Gupta YK and Ahmad S, *J Mater Chem* **B2:** 147–166 (2014).

8. Hoare TR and Kohane DS, *Polymer* **49**: 1993–2007 (2008).

9. Yu L and Ding J, *Chem Soc Rev* **37:** 1473–1481 (2008).

10. Ruel-Gariepy E and Leroux JC, *Eur J Pharm Biopharm* **EV58:** 409–426 (2004).

11. Choi BG*,* Park HP, Cho SH, Oh MK, Kim EH, Park K, Han DK and Jeong B, *Biomaterials* **31**: 9266–9272 (2010).

12. Kabanov AV, Batrakova EV and Alakhov VY, *J Controlled Release* **82:** 189–212 (2002).

13. Kabanov AV and Alakhov VY, *Crit Rev Ther Drug Carrier Syst* **19:** (2002).

14. Khattak SF, Bhatia SR and Roberts SC, *Tissue Eng* **11**: 974–983 (2005).

15. Niu G, Du F, Song L, Zhang H, Yang J, Cao H, Zheng Y, Yang Z, Wang G, Yang H and Zhu S, *J Control Release* **138:** (2009).

16. Volkmer E, Leicht U, Moritz M, Wiese H, Milz S, Matthias P, Schloegl W, Friess W, Goettlinger M, Augat P and Schieker M, *J Mater Sci Mater Med* **24**: 2223–2234 (2013).

17. Sun KH, Sohn YS and Jeong B, *Biomacromolecules* **7**: 2871–2877 (2006).

18. Cohn D, Sosnik A and Levy A, *Biomaterials* **24:** 3707–3714 (2003).

19. Loh XJ, Gan H, Wang H, Tan S, Neoh K, Jean Tan S, Diong H, Kim J, Sharon Lee W, Fang X, Cally O, Yap S, Liong K *and* Chan K, *J Appl Polym Sci* **131**: (2014).

20. Park D, Wu W and Wang YA, *Biomaterials* **32**: 777–786 (2011).

21. Sartori S, Boffito M, Serafini P, Caporale A, Silvestri A, Bernardi E, Sassi MP, Boccafoschi F and Ciardelli G, *React Funct Polym* **73:** 1366–1376 (2013).

22. Pradal C, Jack KS, Grøndahl L and Cooper-White JJ, *Biomacromolecules* **14**: 3780–3792 (2013).

23. Alexandridis P, Holzwarth JF and Hatton TA, *Macromolecules* **27:** 2414–2425 (1994).

24. Gong C, Shi S, Dong P, Kan B, Gou M, Wang X, Li X, Luo F, Zhao X, Wei Y and Qian Z, *Int J Pharm* **365**: 89–99 (2009).

25. Gong CY, Shi S, Dong P, Zheng XL, Fu SZ, Guo G, Yang JL, Wei YQ and Qian ZY, *BMC Biotechnol* **9**: (2009).

26. Boffito M, Sirianni P, Di Rienzo AM and Chiono V, *J Biomed Mater Res* **A103**: 1276–1290 (2015).

27. Bhattacharya M, Malinen MM, Lauren P, Lou YR, Kuisma SW, Kanninen L, Lille M, Corlu A, GuGuen-Guillouzo C, Ikkala O, Laukkanen A, Urtti A, Yliperttula M, *J Control Release* **164:** 291–298 (2012).

28. Ma G, Miao B and Song C, *J Appl Polym Sci* **116**: 1985–1993 (2010).

29. Ranzato E, Patrone M, Mazzucco L and Burlando B, *Br J Dermatol* **159**: 537–545 (2008).

30. Ranzato E, Balbo V, Boccafoschi F, Mazzucco L and Burlando B, *Cell Biol Int* **33**: 911–917 (2009).

31. Ranzato E, Martinotti S and Burlando B, *Burns & Trauma* **1**: 32–38 (2013).

32. Ranzato E, Martinotti S and Burlando B, *J Ethnopharmacol* **134**: 443–449 (2011).

33. Altinok H, Yu GA, Nixon SK, Gorry PA, Attwood D and Booth C, *Langmuir* **13**: 5837–5848 (1997).

34. Kabanov AV, Nazarova IR, Astafieva IV, Batrakova EV, Alakhow VY, Yaroslavov AA and Kabanov VA, *Macromolecules* **28**: 2303–2314 (1995).

35. Brown W, Schillen K and Hvidt S, *J Phys Chem* **96**: 6038–6044 (1992).

36. Dey J, Kumar S, Nath S, Ganguly R, Aswal VK and Ismail K, *J Colloid Interface Sci* **415:** (2014).

37. Pragatheeswaran AM and Chen SB, *Langmuir* **29**: 9694–9701 (2013).

38. Gilbert JC, Richardson JL, Davies MC, Palin KJ and Hadgraft J, *J Controlled Release* **5:** 113–118 (1987).

39. Kwon KW, Park MJ, Hwang J and Char K, *Polymer* **J33**: 404–410 (2001).

40. Pandit NK and Kisaka J, *Int J Pharm* **145**: 129–136 (1996).

41. Doi M and Edwards SF, *Oxford Science Publications* (1986).

42. Wang P and Johnston TP, *J Appl Polym Sci* **43**: 283–292 (1991).

43. Mortensen K, Brown W and Joergensen E, *Macromolecules* **27**: 5654–5666 (1994).

44. Murphy SV and Atala A, *Nat Biotech* **32**: 773–785 (2014).

45. Cui X, Boland T, D'Lima DD and Lotz MK, *Recent Pat Drug Deliv Formul* **6**: 149–155 (2012).

46. Murphy SV, Skardal A and Atala A, *J Biomed Mater Res A* **101A**: 272–284 (2013).

47. Wang W, Liu Z, Sun P, Fang C, Fang H, Wang Y, Ji J and Chen J, *Int J Mol Sci* **16**: 16263-16274 (2015).

48. Kim JY, Choi W, Kim YH and Tae G, *Biomaterials* **34**: 1170-1178 (2013).

TABLE

Table 1. Values levels of statistical significance.

p value	Wording	Summary
< 0.0001	Extremely significant	****
0.0001 to 0.001	Extremely significant	***
0.001 to 0.01	Very significant	**
0.01 to 0.05	Significant	*
≥ 0.05	Not significant	ns

Table 2. CMT values obtained for NHP407 and P407 solutions.

	P407	**NHP407**
Concentration (%w/v)	**CMT (°C)***	
0.1	29	24
0.5	25	23
1	23	22
3	21	20
5	19	18
6	18	17

* error ± 1°C

Table 3. LCGT and UCGT values for P407- and NHP407-based solutions in PBS.

		Concentration (%w/v)																	
		5	**6**	**7**	**8**	**9**	**10**	**12**	**15**	**17**	**18**	**19**	**20**	**22**	**25**	**28**	**30**	**32**	**35**
P407	LCGT (°C)*	-	-	-	-	-	-	-	-	-	29	26	24	22	20	17	16	15	14
	UCGT (°C)*	-	-	-	-	-	-	-	-	-	48	54	56	60	67	(*)	(*)	(*)	(*)
NHP407	LCGT (°C)*	-	45	41	36	34	32	30	26	(**)	23	(**)	22	21	20	(**)	(**)	(**)	(**)
	UCGT (°C)*	-	60	67	69	(*)	(*)	(*)	(*)	(**)	(*)	(**)	(*)	(*)	(*)	(**)	(**)	(**)	(**)

* error ± 0.5°C
(*) UCGT is higher than 70°C
(**) not analyzed sample

Table 4. T_{onset}, T_{gel}, viscosity and LCGT of NHP407 hydrogels with different concentrations.

Concentration %w/v	rheological tests				tube inverting tests
	η_{onset} (Pa s)	T_{onset} (°C)	η_{max} (Pa s)	T_{max} (°C)	LCGT (°C)*
10	0.027	19.0	56	31.8	32.0
15	0.199	15.4	238	26.4	26.0
20	0.488	11.0	316	23.4	22.0

* error ± 0.5°C

Table 5. Yield stress (YS) and strain at peak (γ_{max}) of NHP407 and P407 solutions in PBS at 37°C.

	YS (Pa)	γ_{max} (%)		YS (Pa)	γ_{max} (%)
NHP407_10%w/v	300	18	**P407_10%w/v**	**NA	**NA
NHP407_15%w/v	1500	20	**P407_15%w/v**	**NA	**NA
NHP407_20%w/v	3500	20	**P407_20%w/v**	200	3.6

* The yield stress and the maximum strain value were evaluated at the maximum of loss modulus.
** No gelling system.

Table 6. Domain spacing of NHP407-based hydrogels at different temperatures.

	T (°C)	*$G'_{plateau}$ (Pa)	a^2b (nm^3)
NHP407_10%w/v	37	448	9549
	40	633	6824
	42	730	5955
	45	847	5180
	50	920	4850
NHP407_15%w/v	37	18400	232
	40	21700	199
NHP407_20%w/v	37	39800	107
	40	43200	100

* at 100 rad/s

Table7. Main achievements of the work

	NHP407	**P407**
Molecular weight	26000-35000 Da	12600 Da
Critical Micelle Temperature	0.5%w/v: 23±1 °C 1%w/v: 22±1 °C 3%w/v: 20±1 °C 4%w/v: 18±1 °C 6%w/v: 17±1 °C	0.5%w/v: 25±1 °C 1%w/v: 23±1 °C 3%w/v: 21±1 °C 4%w/v: 19±1 °C 6%w/v: 18±1 °C
Average micelle size at 25 °C *(dynamic light scattering)*	0.5%w/v: 46.0±6.9 nm 1%w/v: 88.9±10.3 nm	0.5%w/v: 24.0±0.8 nm 1%w/v: 28.2±0.3 nm
Critical Gelation Concentration	6±1 %w/v	18±1 %w/v
Gelation Temperature (tube inverting test)	10%w/v: 32±0.5 °C 15%w/v: 26±0.5 °C 20%w/v: 22±0.5 °C	10%w/v: no gelation 15%w/v: no gelation 20%w/v: 24±0.5 °C
Gel viscosity	10%w/v: 56 Pa s 15%w/v: 238 Pa s 20%w/v: 316 Pa s	10%w/v: no gelation 15%w/v: no gelation 20%w/v: 16 Pa s
Resistance to deformation at 37°C (strain value at the maximum of G'')	10%w/v: 18% 15%w/v: 20% 20%w/v: 20%	10%w/v: no gelation 15%w/v: no gelation 20%w/v: 3.6%
Gel strength G' at 37°C	10%w/v: 448 Pa 15%w/v: 18400 Pa 20%w/v: 39800 Pa	10%w/v: no gelation 15%w/v: no gelation 20%w/v: 12000 Pa
Gelation time at 37°C	10%w/v: <5 minutes 15%w/v: <5 minutes 20%w/v: <5 minutes	10%w/v: no gelation 15%w/v: no gelation 20%w/v: <5 minutes
Stability in aqueous media	Long term stability (up to 28 days)	Fast dissolution (less than 5 days)
Permeability to nutrients	10%w/v: 40.6±0.3 % * 15%w/v: 30.4±0.5 % * 20%w/v: 27.6±1.3 %* *after 7 days	**
Covalent functionalization with peptide sequences or proteins	Covalent grafting to serine amino groups after Boc deprotection	Possible grafting at the chain ends [47,48]
Injectability	10%w/v: injectable 15%w/v: injectable (formation of continuous filaments)	10%w/v: injectable 15%w/v: injectable 20%w/v: injectable

	20%w/v: injectable (formation of continuous filaments)	

** not analyzed samples